Mon. Not. R. Astron. Soc. **000**, 1–11 (2005) Printed 5 February 2008 (MN LATEX style file v2.2)

Relativistic Fermi acceleration with shock compressed turbulence

Martin Lemoine[1⋆] and Benoît Revenu[2,1]†
[1] *Institut d'Astrophysique de Paris,*
UMR 7095 CNRS, Université Pierre & Marie Curie
98 bis boulevard Arago, F-75014 Paris, France
[2] *AstroParticule & Cosmologie,*
UMR 7164 CNRS, Université Denis Diderot

ABSTRACT
This paper presents numerical simulations of test particle Fermi acceleration at relativistic shocks of Lorentz factor $\Gamma_{\rm sh} = 2 - 60$, using a realistic downstream magnetic structure obtained from the shock jump conditions. The upstream magnetic field is described as pure Kolmogorov turbulence; the corresponding downstream magnetic field lies predominantly in the plane tangential to the shock surface and the coherence length is smaller along the shock normal than in the tangential plane. Acceleration is nonetheless efficient and leads to power-law spectra with index $\simeq 2.6 - 2.7$ at large shock Lorentz factor $\Gamma_{\rm sh} \gg 1$, markedly steeper than for isotropic scattering downstream. The acceleration timescale $t_{\rm acc}$ in the upstream rest frame becomes a fraction of Larmor time $t_{\rm L}$ in the ultra-relativistic limit, $t_{\rm acc} \approx 10 t_{\rm L}/\Gamma_{\rm sh}$. Astrophysical applications are discussed, in particular the acceleration in $\gamma-$ray bursts internal and external shocks.

Key words: shock waves – acceleration of particles – cosmic rays

1 INTRODUCTION

The Fermi acceleration process of charged particles bouncing back and forth across a shock wave is the main ingredient for the generation of high energy radiation in a variety of astrophysical environments. This observed radiation is generally synchrotron light emitted by the accelerated electrons; in this case one may recover the spectral index s of the accelerated population from the synchrotron index. For example, the afterglow emission of $\gamma-$ray bursts that is seen in X-ray through the infrared is generally interpreted as synchrotron emission of electrons accelerated at the ultra-relativistic external shock of Lorentz factor $\Gamma_{\rm sh} \sim 300$. The inferred spectral index, $s \simeq 2.3 \pm 0.1$ (Waxman 1997; see also Meszaros 2002 and Piran 2004 for reviews), thus probes the nature of shock acceleration in the ultra-relativistic regime. Similarly synchrotron emission of electrons accelerated in the mildly relativistic internal shocks ($\Gamma_{\rm sh} \sim 2 - 5$ in the comoving frame) with index $s \simeq 2.3 \pm 0.1$ could explain the prompt γ emission (see e.g. Meszaros 2002, Piran 2004 and references therein). These observations thus provide anchor points for studies of Fermi acceleration in the moderate to the ultra- relativistic regime. They have actually been regarded as a dramatic confirmation of the theory of shock acceleration in the relativistic regime, which has been claimed to predict a "universal" asymptotic spectral index $s \simeq 2.23$ in the ultra-relativistic regime $\Gamma_{\rm sh} \gg 1$.

Relativistic shock acceleration has been studied through a variety of methods, either analytical (Peacock 1981, and more recently Vietri 2002, Vietri 2003, Keshet & Waxman 2005, Blasi & Vietri 2005), semi-analytical (Kirk & Schneider 1987; Gallant & Achterberg 1999; Kirk *et al.* 2000; Achterberg *et al.* 2001), or numerical (Ellison *et al.* 1990, Ostrowski 1991, Ballard & Heavens 1992, Ostrowski 1993, Bednarz & Ostrowski 1996, 1998, 1999, Ellison & Double 2002, 2004, Lemoine & Pelletier 2003, Meli & Quenby 2003a,b, Bednarz 2004, Niemec & Ostrowski 2004, Baring 2004). Not all of these studies find the universal value for s, however, all the more so when anisotropic configurations such as oblique shocks are considered. One clear example is the demonstration that Fermi acceleration in superluminal (perpendicular) shocks in the absence of cross-field diffusion becomes inefficient (Begelman & Kirk 1990); in the relativistic regime, oblique shocks are superluminal unless the angle between the magnetic field and the shock normal $\Theta_B \lesssim 1/\Gamma_{\rm sh}$.

It is generally suspected that the inclusion of scattering would make Fermi acceleration more efficient in the relativistic regime. The simulations of Bednarz & Ostrowski (1998) and Baring (2004) have indeed confirmed that the spectral slope tends to increase with increasing shock obliquity and with decreasing turbulence level, whose rôle is to permit cross-field line transport to the shock front. However, a limitation of these simulations is that the scattering is simulated in a phenomenological way by setting a ratio of the perpendicular to parallel diffusion lengths and drawing pitch angles at random at each time step. Upstream, it has been demonstrated that an ultra-relativistic shock wave overtakes the particle before this latter has had time to scatter efficiently (Gallant & Achterberg 1999, Achterberg *et al.* 2001), so that the details of particle trans-

⋆ E-mail: lemoine@iap.fr
† E-mail: revenu@iap.fr

port are probably not crucial. Downstream, however, the particle has to turn back before re-crossing the shock, and the approximation of ad-hoc diffusion lengths may be too naïve to accurately simulate the transport. In fact, one may expect non-trivial correlation functions between displacements along different directions as well as subdiffusion regimes to play a significant rôle in the return to the shock.

Several studies have tried to integrate out exactly the particles trajectories in a well-defined magnetic field structure (Ballard & Heavens 1992, Ostrowski 1993, Lemoine & Pelletier 2003, Niemec & Ostrowski 2004). The study of Ballard & Heavens (1992) involved a realistic magnetic field structure, in the sense that it obeys the shock jump conditions, but was limited to mildly relativistic shocks ($\Gamma_{\rm sh} \leqslant 5$). Nevertheless, it observed a trend of increasing spectral index with increasing shock velocity, a result which has been disputed by the more exhaustive simulations of Ostrowski (1993). The recent work of Niemec & Ostrowski (2004) considered situations of moderate turbulence levels with varying degrees of obliquity for mildly relativistic shocks ($\Gamma_{\rm sh} \leqslant 5$). The conclusions obtained indicate that various spectral slopes can indeed be obtained, although the noise on the simulations is not negligible. Finally, the work of Lemoine & Pelletier (2003) introduced a new numerical Monte Carlo method to study relativistic Fermi acceleration, on which the present work is based. It assumed the downstream turbulence to be isotropic and confirmed the value $s \simeq 2.2-2.3$ predicted in that case.

It seems fair to say that a clear picture of the efficiency of relativistic Fermi acceleration in a magnetic structure that includes compression of the upstream magnetized configuration has not yet emerged. The present paper proposes to undertake such simulations in order to make progress along these lines. We assume that the upstream magnetic field is described by pure Kolmogorov turbulence, i.e. there is not uniform component; this can be seen as the limit $\delta B/B \to \infty$ of a highly turbulent plasma. The upstream magnetic field is compressed by the shock into an anisotropic downstream turbulence. We conduct our simulations in the mildly and ultra-relativistic regimes; simulations of that kind in this latter regime have never been attempted before.

In Section 2, we describe in detail the numerical techniques and the procedure used (borrowed from Lemoine & Pelletier 2003) to simulate the Fermi acceleration process. In Section 3, we present our results on the (downstream) return probability, the acceleration timescale and the accelerated spectrum as a function of shock Lorentz factor. In Section 4 we discuss the relaxation length of the turbulence and argue that, for relativistic shocks at least, particles that return to the shock downstream do not travel beyond the point where the anisotropy of turbulence has relaxed. We also discuss the properties of transport of particles in the strongly anisotropic turbulence generated by shock compression, compare our results to previous studies and comment on the applications of our results to shock acceleration in $\gamma-$ray bursts and to shock acceleration of ultra-high energy cosmic rays. Conclusions and a summary of the results are provided in Section 5.

2 NUMERICAL SIMULATIONS

2.1 Jump conditions and magnetic fields

In the present work, we assume that the magnetic field is dynamically unimportant, *i.e.* its energy density can be neglected with respect to that of the fluid. We also consider a strong shock, for which the upstream random kinetic energy per particle can be neglected with respect to that downstream. The corresponding hydrodynamic jump conditions are given in Blandford & McKee (1977), and reviewed in Kirk & Duffy (2001) and Gallant (2002). The shock Lorentz factor is denoted $\Gamma_{\rm sh}$ in the upstream frame (taken as the lab frame), and the shock velocity upstream is $\beta_{\rm sh}$. Unless otherwise noted, all quantities are calculated in this frame. If relevant the reference frame is indicated by a subscript, e.g., $\beta_{\rm sh|d}$ refers to the shock velocity measured in the downstream rest frame and $\Gamma_{\rm sh|d}$ refers to the shock Lorentz factor in the downstream frame. The relative Lorentz factor between upstream and downstream is noted $\Gamma_{\rm rel}$ and reads:

$$\Gamma_{\rm rel} \equiv \Gamma_{\rm sh}\Gamma_{\rm sh|d}(1-\beta_{\rm sh}\beta_{\rm sh|d}).$$

The downstream Lorentz factor $\Gamma_{\rm sh|d}$ as well as $\Gamma_{\rm rel}$ can be obtained as a function of $\Gamma_{\rm sh}$ (upstream shock Lorentz factor) using the relations derived from the shock jump conditions for a Synge equation of state (Gallant 2002):

$$\Gamma^2_{\rm sh|d} \,=\, \frac{F(\xi)}{F(\xi)-1}\,, \quad \Gamma^2_{\rm sh} \,=\, G(\xi)^2\frac{F(\xi)}{F(\xi)-1} \qquad (1)$$

where $\xi \equiv mc^2/T_{\rm d}$, $T_{\rm d}$ being the downstream temperature and m the particle mass, $G(\xi) \equiv K_3(\xi)/K_2(\xi)$, with K_2, K_3 modified Bessel functions, and $F(\xi) \equiv \left[\xi G(\xi)-1\right]^2 - \xi^2$. These relations hold for a gas composed of possibly different particles species but with same ξ (Gallant 2002). Equations (1) can be inverted numerically to obtain $\Gamma_{\rm sh|d}$ as a function of $\Gamma_{\rm sh}$. In particular, in the ultra-relativistic limit $\Gamma_{\rm sh} \to +\infty$, one finds the well-known results $\beta_{\rm sh|d} \to 1/3$ ($\Gamma_{\rm sh|d} \to 3/\sqrt{8}$) and $\Gamma_{\rm rel} \to \Gamma_{\rm sh}/\sqrt{2}$.

The conservation of the electromagnetic field energy-momentum tensor implies the following jump conditions for the magnetic field components $B_\parallel$ (aligned with the shock normal) and $B_\perp$ (tangential to the shock surface):

$$\frac{B_{\parallel,{\rm d|d}}}{B_{\parallel,{\rm u|u}}} \,=\, 1, \qquad \frac{B_{\perp,{\rm d|d}}}{B_{\perp,{\rm u|u}}} \,=\, \frac{\beta_{\rm sh|u}\Gamma_{\rm sh|u}}{\beta_{\rm sh|d}\Gamma_{\rm sh|d}}, \qquad (2)$$

and as before, $\beta_{\rm sh|u} \equiv \beta_{\rm sh}$, $\Gamma_{\rm sh|u} \equiv \Gamma_{\rm sh}$. The parallel component $B_\parallel$ is thus conserved while the perpendicular component $B_\perp$ is amplified by the proper shock compression ratio $R = \beta_{\rm sh|u}\Gamma_{\rm sh|u}/\beta_{\rm sh|d}\Gamma_{\rm sh|d}$. In the ultra-relativistic limit $R \to \Gamma_{\rm sh}\sqrt{8}$, and the total magnetic field strength is amplified by $\sqrt{2/3}R$.

We assume that the upstream magnetic field is purely turbulent with a power spectrum describing Kolmogorov turbulence with maximal length scale $L_{\rm max}$. It is modeled as a sum of static plane wave modes according to:

$$\mathbf{B}_{\rm u}(\mathbf{x}) \,=\, \sum_{\mathbf{k}} \, e^{i\mathbf{k}\cdot\mathbf{x}+i\phi_{\mathbf{k}}}\,\mathbf{e}_{\mathbf{k}}G_k, \qquad (3)$$

with $\mathbf{e}_{\mathbf{k}}$ a unit polarization vector orthogonal to $\mathbf{k}$, $\phi_{\mathbf{k}}$ a random phase and $|G_k|^2 \,\propto\, k^{-5/3}$ the amplitude of the power spectrum. The wavenumbers k range from $k_{\rm min} = 2\pi/L_{\rm max}$ to some maximal wavenumber $k_{\rm max} \gg k_{\rm min}$; numerically we employ 250 wavenumbers modes whose directions are drawn at random, and whose moduli are spaced logarithmically between $k_{\rm min}$ and $k_{\rm max} = 5\cdot 10^3 k_{\rm min}$. The amplitude G_k can be chosen as real and is normalized such that:

$$\frac{1}{V}\int {\rm d}\mathbf{x}\,\mathbf{B}^2(\mathbf{x}) \,=\, \sum_{\mathbf{k}}|G_k|^2 \,\equiv\, B^2_{\rm rms} \qquad (4)$$

with $B^2_{\rm rms}$ the squared turbulent magnetic field strength.

According to the shock jump conditions, the downstream

magnetic field is described by an anisotropic turbulence: while $B_\parallel$ is conserved, the turbulence wavenumbers $k_\parallel$ are amplified by R, which corresponds to the compression of the eddies by $1/R$ along the shock normal. The perpendicular wavenumbers $k_\perp$ are conserved through the shock but $B_\perp$ is amplified as before. Hence the downstream magnetic field is described by:

$$\mathbf{B}_{\rm d}(\mathbf{x}) \,=\, \sum_{\tilde{\mathbf{k}}} \, e^{i\tilde{\mathbf{k}}\cdot\mathbf{x}+i\phi_{\tilde{\mathbf{k}}}} \, \tilde{\mathbf{e}}_{\tilde{\mathbf{k}}} G_k, \tag{5}$$

where $\tilde{\mathbf{k}}$ is related to the wavenumber $\mathbf{k}$ of Eq. 3 by $\tilde{\mathbf{k}}_\parallel = R\,\mathbf{k}_\parallel$ and $\tilde{\mathbf{k}}_\perp = \mathbf{k}_\perp$; similarly $\tilde{\mathbf{e}}_{\mathbf{k}}$ is related to $\mathbf{e}_{\mathbf{k}}$ by: $\tilde{\mathbf{e}}_{\parallel,\mathbf{k}} = \mathbf{e}_{\parallel,\mathbf{k}}$ and $\tilde{\mathbf{e}}_{\perp,\mathbf{k}} = R\,\mathbf{e}_{\perp,\mathbf{k}}$. Note that $\tilde{\mathbf{k}}\cdot\tilde{\mathbf{e}}_{\tilde{\mathbf{k}}} = \mathbf{k}\cdot\mathbf{e}_{\mathbf{k}} = 0$ as required for a divergenceless field; $\phi_{\tilde{\mathbf{k}}}$ and G_k are not modified. We chose not to normalize the above polarization vector to unity downstream and its modulus gives the overall amplification factor of the magnetic field. This is but a matter of convention: one may equally well embody the compression factor in G_k and normalize $\tilde{\mathbf{e}}_{\tilde{\mathbf{k}}}$ to unity.

2.2 Monte Carlo simulations

Our numerical procedure is summarized in Lemoine & Pelletier (2003). It consists in two main steps: in a first stage, we conduct Monte Carlo simulations of particle propagation in a magnetized medium (either upstream or downstream) and derive the statistical properties related to shock crossing and re-crossing, as described below. In a second step we use these statistical distributions in conjunction with the Lorentz transforms from one frame to the other to reconstruct the accelerated spectrum that escapes downstream.

Once the magnetic field structure is set up as described above, one Monte Carlo simulation of the propagation of particle consists in integrating the equation of motion in the magnetic field. The particle trajectory is saved in time intervals that are a fraction $f_{\rm u} \simeq 10^{-4}$ (upstream) or $f_{\rm d} \simeq 10^{-2}$ (downstream) of Larmor time $t_{\rm L} = R_{\rm L}/c$ (with $R_{rmL} \equiv p/qB$) over a time period as long as $\Delta T_{\rm u} \simeq 10^2$ (upstream) or $\Delta T_{\rm d} \simeq 10^4$ (downstream) Larmor time. For each computed trajectory one can build a statistical sample of shock crossing and re-crossing as follows. One draws at random a point along the trajectory, which defines the point at which the particle enters through the shock. One records the ingress pitch angle cosine of the particle momentum with respect to the shock normal at that point. One then searches for the point along the trajectory at which the particle exits through the shock and the corresponding egress pitch angle cosine is recorded. In the downstream medium, it happens that the particle never re-crosses the shock as the shock itself moves away with speed $\beta_{\rm sh|d} \simeq 1/3$ ($\Gamma_{\rm sh} \gg 1$). By iterating the above procedure, *i.e.* drawing other points of entry in the trajectory, and building other trajectories, one can measure the probability laws that control in a direct manner the Fermi process.

In particular, the ratio of the number of shock re-crossings to the total number of shock entries at a given ingress "pitch" angle (defined here as the angle between the momentum and the direction of the shock normal) cosine $\mu^{\rm i}$ gives the return probability $P_{\rm ret}(\mu^{\rm i})$. In a similar way, the number of shock re-crossings through an egress pitch angle cosine $\mu^{\rm e}$ for a given ingress cosine $\mu^{\rm i}$ gives (after proper normalization) the conditional return probability $\mathcal{P}(\mu^{\rm i};\mu^{\rm e})$. One can define and calculate these quantities both downstream, $\mathcal{P}_{\rm d}(\mu^{\rm i}_{\rm d};\mu^{\rm e}_{\rm d})$, and upstream, $\mathcal{P}_{\rm u}(\mu^{\rm i}_{\rm u};\mu^{\rm e}_{\rm u})$. Note that the ingress and egress pitch angles are calculated in the rest frame of the fluid under consideration. The normalization of the conditional probability laws is such that their sum over the egress pitch angle cosine yields the return probability as a function of ingress pitch angle cosine:

$$\begin{aligned} P_{\rm ret,\,d}(\mu^{\rm i}_{\rm d}) \;&=\; \int {\rm d}\mu^{\rm e}_{\rm d}\, \mathcal{P}_{\rm d}(\mu^{\rm i}_{\rm d};\mu^{\rm e}_{\rm d}), \\ P_{\rm ret,\,u}(\mu^{\rm i}_{\rm u}) \;&=\; \int {\rm d}\mu^{\rm e}_{\rm u}\, \mathcal{P}_{\rm u}(\mu^{\rm i}_{\rm u};\mu^{\rm e}_{\rm u}). \end{aligned} \tag{6}$$

Obviously the upstream return probability $P_{\rm ret,\,u}$ must be unity if one considers an infinite planar shock with an infinite lifetime. This provides a useful check on the numerical procedure; in the present calculations, $P_{\rm ret,\,u}$ does not deviate from unity by more than $\sim 10^{-6}$. Downstream it is mandatory to verify that one does not miss possible late returns by varying the trajectory integration time; we estimate that the mean of $P_{\rm ret,\,d}$ over ingress pitch angle cosines is accurate to better than $\sim 10^{-4}$.

Finally these simulations give a direct measurement of the return timescale to the shock as a function of pitch angles. This measurement is particularly important to estimate the maximal acceleration energy in a variety of environments, as discussed in Section 3.3.

Once the upstream and downstream laws of return probability are known, the simulation of the acceleration process itself can be performed as follows. We denote by $\mathcal{F}^{2n+1}_{\rm d}(\mu_{\rm d},\epsilon_{\rm d})$ the distribution function of particles that enter the shock towards downstream with ingress pitch angle cosine $\mu_{\rm d}$, that have experienced $2n+1$ shock crossings and that carry energy $\epsilon_{\rm d}$ (downstream frame). Similarly we define the distribution function $\mathcal{F}^{2n}_{\rm u}(\mu_{\rm u},\epsilon_{\rm u})$ of upstream-going particles with ingress pitch angle cosine $\mu_{\rm u}$, having experienced $2n$ shock crossings and carrying energy $\epsilon_{\rm u}$. If we denote by $\mathcal{F}^0_{\rm u}$ the injection population upstream, then after an even (resp. odd) number of shock crossings the particles are necessarily upstream (resp. downstream). The injection (isotropic) distribution function $\mathcal{F}^0_{\rm u}$ is normalized to unity, as follows:

$$\int_{-1}^{1} {\rm d}\mu_{\rm u}{\rm d}\epsilon_{\rm u}\, \mathcal{F}^0_{\rm u}(\mu_{\rm u},\epsilon_{\rm u}) \,\equiv\, 1. \tag{7}$$

The integral over μ and ϵ of the distribution functions $\mathcal{F}^{2n+1}_{\rm d}(\mu,\epsilon)$ and $\mathcal{F}^{2n}_{\rm u}(\mu,\epsilon)$ with $n>0$ is smaller than unity, due to escape of particles downstream at each cycle.

Now, particles that enter upstream after $2n$ shock crossings with ingress cosine $\mu^{\rm i}_{\rm u}$ re-cross the shock with egress cosine $\mu^{\rm e}_{\rm u}$ and with conditional probability $\mathcal{P}_{\rm u}(\mu^{\rm i}_{\rm u};\mu^{\rm e}_{\rm u})$. The total number of particles with egress pitch angle $\mu^{\rm e}_{\rm u}$ and energy $\epsilon_{\rm u}$ at the $2n+1^{\rm th}$ shock crossing is $\int {\rm d}\mu^{\rm i}_{\rm u}\, \mathcal{P}_{\rm u}(\mu^{\rm i}_{\rm u};\mu^{\rm e}_{\rm u}) \mathcal{F}^{2n}_{\rm u}(\mu^{\rm i}_{\rm u},\epsilon_{\rm u})$. We note that the upstream egress cosine $\mu^{\rm e}_{\rm u}$ is related to the corresponding downstream ingress cosine $\mu^{\rm i}_{\rm d}$, by a Lorentz transform, just as the energies measured in the upstream frame ($\epsilon_{\rm u}$) or downstream frame ($\epsilon_{\rm d}$):

$$\mu^{\rm i}_{\rm d} \,=\, \frac{\mu^{\rm e}_{\rm u}-\beta_{\rm rel}}{1-\beta_{\rm rel}\mu^{\rm e}_{\rm u}}, \quad \epsilon_{\rm d} \,=\, \Gamma_{\rm rel}(1-\beta_{\rm rel}\mu^{\rm e}_{\rm u})\epsilon_{\rm u}, \tag{8}$$

with a similar relation between $\mu^{\rm e}_{\rm d}$ and $\mu^{\rm i}_{\rm u}$ when the particle crosses the shock from downstream to upstream.

Therefore, the conservation of particle number at shock crossing u→d implies the following relation between $\mathcal{F}^{2n+1}_{\rm d}$ and $\mathcal{F}^{2n}_{\rm u}$:

$$\begin{aligned} &\mathcal{F}^{2n+1}_{\rm d}(\mu^{\rm i}_{\rm d},\epsilon_{\rm d})\,{\rm d}\mu^{\rm i}_{\rm d}{\rm d}\epsilon_{\rm d} = \\ &\qquad \left[\int_{\beta_{\rm sh}}^{1} {\rm d}\mu^{\rm i}_{\rm u}\, \mathcal{P}_{\rm u}(\mu^{\rm i}_{\rm u};\mu^{\rm e}_{\rm u}) \mathcal{F}^{2n}_{\rm u}(\mu^{\rm i}_{\rm u},\epsilon_{\rm u})\right] {\rm d}\mu^{\rm e}_{\rm u}{\rm d}\epsilon_{\rm u}, \end{aligned} \tag{9}$$

and one obtains a similar system for shock crossing d→u:

$$\mathcal{F}_{\rm u}^{2n}(\mu_{\rm u}^{i},\epsilon_{\rm u})\,{\rm d}\mu_{\rm u}^{\rm i}{\rm d}\epsilon_{\rm u} = \left[\int_{-1}^{\beta_{\rm sh|d}} {\rm d}\tilde{\mu}_{\rm d}^{\rm i}\,\mathcal{P}_{\rm d}(\tilde{\mu}_{\rm d}^{\rm i};\mu_{\rm d}^{\rm e})\mathcal{F}_{\rm d}^{2n-1}(\tilde{\mu}_{\rm d}^{\rm i},\tilde{\epsilon}_{\rm d})\right]\,{\rm d}\mu_{\rm d}^{\rm e}{\rm d}\tilde{\epsilon}_{\rm d}, \quad (10)$$

with:

$$\mu_{\rm u}^{\rm i} \,=\, \frac{\mu_{\rm d}^{\rm e}+\beta_{\rm rel}}{1+\beta_{\rm rel}\mu_{\rm d}^{\rm e}}, \quad \epsilon_{\rm u} \,=\, \Gamma_{\rm rel}(1+\beta_{\rm rel}\mu_{\rm d}^{\rm e})\tilde{\epsilon}_{\rm d} \quad (11)$$

where the " $\tilde{}$ " symbol has been introduced to differentiate the values of $\mu_{\rm d}$ and $\epsilon_{\rm d}$ from one cycle ($2n-1$ shock crossings) to the next ($2n+1$ shock crossings). The integration bounds on μ are imposed by the shock crossing conditions.

The terms within brackets in Eqs. (9) and (10) correspond to the distributions upon exit from upstream and downstream respectively. These equations assume implicitly that the conditional probability laws do not depend on energy. This will be shown to be a good approximation in Section 3.1.

After each cycle u→d→u, a population $\mathcal{F}_{\rm out}^{2n+1}(\epsilon_{\rm d}) = \int {\rm d}\mu_{\rm d}^{\rm i}[1-P_{\rm ret}(\mu_{\rm d}^{\rm i})]\mathcal{F}_{\rm d}^{2n+1}(\mu_{\rm d}^{\rm i};\epsilon_{\rm d})$ of the particle population has escaped downstream. The sum over n of these escaping particles forms the outgoing accelerated particle population:

$$\mathcal{F}_{\rm out}(\epsilon) \,=\, \sum_{n=0}^{n=+\infty} \mathcal{F}_{\rm out}^{2n+1}(\epsilon). \quad (12)$$

By following each shock crossing, and using Eqs. (8), (9), (10), (11) and (12) one can follow the evolution of $\mathcal{F}_{\rm d}$, $\mathcal{F}_{\rm u}$ and $\mathcal{F}_{\rm out}$, starting from a mono-energetic and isotropic initial injection distribution upstream. A similar formal development of the acceleration process by repeated shock crossings has also been proposed independently by Vietri (2002): the flux of particles crossing the shock in the stationary regime, noted $J_{\rm in}$ in Vietri (2002) is related to the above as $J_{\rm in} = C\sum_{n=0}^{n=+\infty}\mathcal{F}_{\rm d}^{2n+1}$ with C a normalization constant (see also Lemoine & Pelletier 2003).

The present technique has significant advantages when compared to standard Monte Carlo techniques which follow the particle trajectories on both sides of the shock through the whole acceleration process; in particular, it offers a significant gain in signal to noise as will be obvious in Section 3.

It has however one caveat that should be underlined and which resides in the fact that we compute the accelerated spectrum by merging separate pieces of information on transport properties upstream and downstream. In so doing, we neglect the possible correlations that may exist between the upstream magnetic configuration at the crossing point and that downstream, i.e. we neglect the possible correlations between upstream and downstream transport. The only method that can take this effect into account is the direct Monte Carlo integration of individual particle trajectories. It is therefore important to compare the results obtained with these two methods in order to assess the magnitude of this effect. In the case where scattering is isotropic downstream, it appears that various methods converge to the same value of the spectral index, and this includes various non-Monte Carlo methods which cannot take the above effect into account (see, e.g., Achterberg *et al.* 2001, Lemoine & Pelletier 2003, Keshet & Waxman 2005) as well as direct Monte Carlo methods (e.g., Bednarz & Ostrowski 1998). This suggests that, at least in the isotropic limit, these correlations do not play a significant rôle in the determination of the spectral index.

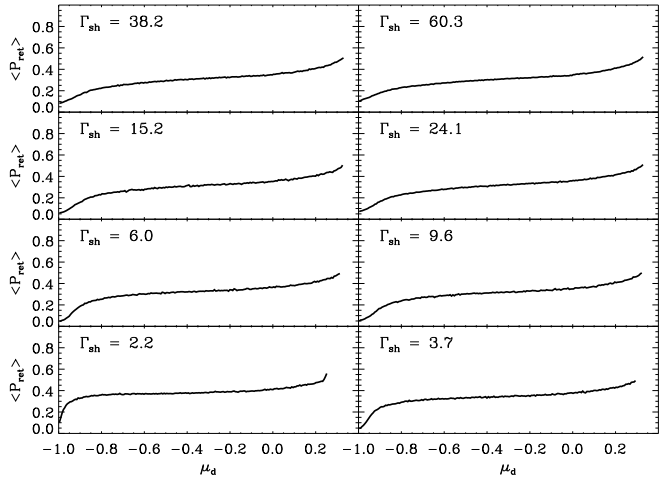

Figure 1. Downstream return probability *vs* ingress pitch angle cosine μ_d^i (downstream rest frame) for various shock Lorentz factors, as indicated, and for a rigidity $2\pi R_{\rm L}/L_{\rm max} = 6\cdot 10^{-4}$.

3 RESULTS

The numerical technique described in the previous section allows to collect a significant amount of information on the acceleration process, in particular the conditional probabilities of return from downstream or upstream, the energy gain per cycle as well as the acceleration timescale. In order to better understand the results obtained for each of these quantities, it is necessary to emphasize the difference between the effective coherence length along the shock normal $L_\parallel$ and that tangential to the shock front $L_\perp$ as measured downstream, see Section 2: $L_\parallel = L_\perp/R = L_{\rm max}/R$, where $L_{\rm max}$ is the coherence length of the upstream magnetic field, and R the proper shock compression ratio, $R \simeq \Gamma_{\rm sh}\sqrt{8}$ when $\Gamma_{\rm sh} \gg 1$. This distinction takes on a particular importance when one compares the results over various values of the shock Lorentz factor and over various values of the rigidity $\rho \equiv 2\pi R_{\rm L}/L_{\rm max}$, where $R_{\rm L}$ denotes the Larmor radius in the rest frame of consideration. In principle, the transport properties of particles in a magnetic field depend solely on the rigidity. However, when the effective coherence length along the shock normal depends on $\Gamma_{\rm sh}$ through R, while $L_\perp$ does not, there is no unambiguous definition of rigidity. In particular, the above definition of ρ does not correspond to the effective rigidity $\rho_\parallel \equiv 2\pi R_{\rm L}/L_\parallel$ that controls the scattering of particles with turbulence modes of wavevector parallel to the shock normal: a given rigidity $\rho = 2\pi R_{\rm L}/L_{\rm max}$ corresponds in fact to larger and larger values of $\rho_\parallel$ as $\Gamma_{\rm sh}$ increases. The relevance of this observation to the results will be adressed shortly.

3.1 Return probability

The average return probability marginalized over egress angle, $P_{\rm ret,d}$, defined in Eq. 6 as the direct average of the conditional probability law $\mathcal{P}_{\rm d}(\mu_{\rm d}^{\rm i},\mu_{\rm d}^{\rm e})$ over the egress pitch angle cosine $\mu_{\rm d}^{\rm e}$, is shown as a function of the ingress pitch angle cosine $\mu_{\rm d}^{\rm i}$ in Fig. 1. The increase of $P_{\rm ret,d}$ as $\mu_{\rm d}^{\rm i} \to 1/3$ backs up the notion that particles crossing the shock from upstream to downstream at near grazing incidence with the shock front have a substantially higher probability of returning to the shock than those crossing the shock head-on ($\mu_{\rm d}^{\rm i} \to -1$).

When viewed as a function of shock Lorentz factor, the av-

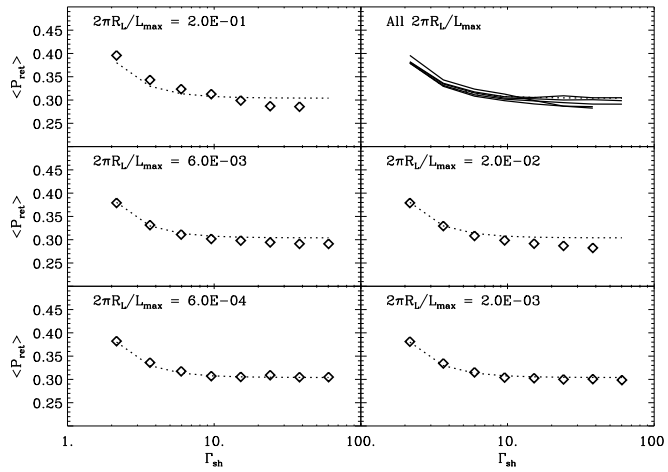

Figure 2. Downstream return probability averaged over ingress angle *vs* shock Lorentz factors for various rigidities as indicated. The dotted line is an ad-hoc fit $\langle P_{\rm ret}\rangle = 0.97 - 0.67\beta_{\rm sh}$ which accounts well for the dependence of the return probability with shock Lorentz factor at low rigidities.

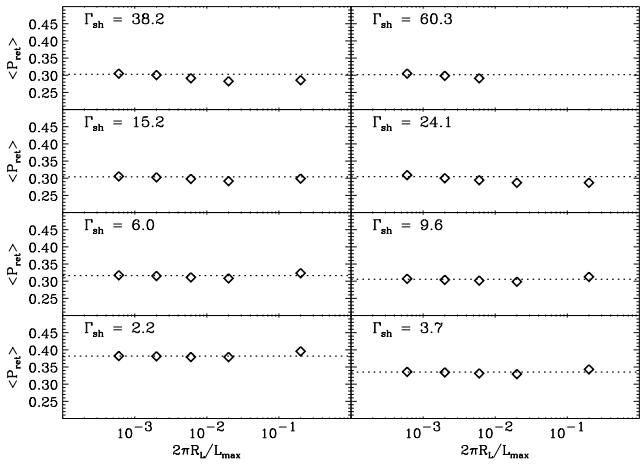

Figure 3. Downstream return probability averaged over ingress angle *vs* rigidity for various shock Lorentz factors, as indicated.

erage return probability appears to reach an asymptotic law, as is made apparent in Fig. 1. This is not a trivial result in itself, as the nature of the turbulence downstream depends rather strongly on the shock Lorentz factor. Section 4.1 provides examples of downstream trajectories for two different values of $\Gamma_{\rm sh}$, and indeed, the displacements along the shock normal differ widely. Hence one might naturally expect that the return probability would carry some form of dependence on the shock Lorentz factor $\Gamma_{\rm sh}$. As we now argue, this is related to the fact that the scattering timescale in the direction along the shock normal, i.e. the time required for the particle to turn back, is a function of Larmor time, as demonstrated in Section 4.1. There it is argued that the particles that return to the shock have done one reflection on the compressed turbulence in their first interaction; indeed, particles get trapped in a layer of the compressed turbulence when $\Gamma_{\rm sh} \gg 1$ and $\rho \ll 1$, hence they cannot return to the shock unless they do so in the first interaction. This reflection is in fact a half-gyration of the particle around a field line which is mainly oriented along the shock front as a result of shock compression, and this explains why the scattering time is of order of the Larmor time. For large values of $\Gamma_{\rm sh}$, the shock velocity with respect to downstream $\beta_{\rm sh|d} \rightarrow 1/3$ becomes independent of $\Gamma_{\rm sh}$, and so does the scattering timescale (at a given rigidity, see Section 4.1), hence so does the return probability.

One may further average the return probability $P_{\rm ret,d}$ over the ingress pitch angle in order to define the average return probability $P_{\rm ret}$:

$$\langle P_{\rm ret}\rangle \equiv \frac{\int {\rm d}\mu_{\rm d}^{\rm i}\, P_{\rm ret,d}(\mu_{\rm d}^{\rm i})}{\int {\rm d}\mu_{\rm d}^{\rm i}}. \qquad (13)$$

This probability is shown as a function of shock Lorentz factor for varying values of the rigidity ρ in Fig. 2. The dotted line represents the empirical fit: $\langle P_{\rm ret}\rangle \simeq 0.97 - 0.66\beta_{\rm sh}$ which provides a good approximation at low rigidities. This figure shows how the average return probability reaches an asymptote with $\Gamma_{\rm sh}$ for sufficiently low rigidities. At high rigidities (upper panels), one recovers a dependence of $\langle P_{\rm ret}\rangle$ on $\Gamma_{\rm sh}$. This latter effect is likely related to the factor R difference between $\rho_\parallel$ and ρ: as $\rho_\parallel = R\rho$ becomes larger than $\approx 0.1 - 1$, particles can no longer interact resonantly with the turbulence wave modes (Casse *et al.* 2002); they take a longer time to return to the shock, see Section 3.3, and their return probability becomes sensitive to the nature of the turbulence, hence to $\Gamma_{\rm sh}$.

Finally one can plot the average return probability as a function of rigidity for various values of the shock Lorentz factor, see Fig. 3. It is important to note that the average return probability does not depend on the rigidity, at least for sufficiently low rigidities $\rho_\parallel \ll 1$ for the same reasons as above. The conditional return probabilities (from which $\langle P_{\rm ret}\rangle$ is obtained) are also found not to depend on rigidity in that range. In order to measure the spectral index of the accelerated spectrum for rigidities in the inertial range of resonance, it is important to use only the datasets of the smallest rigidities downstream, i.e. $\rho = 6\cdot 10^{-4}$ and $\rho = 2\cdot 10^{-3}$, where we still have $k_{\rm max}R_{\rm L} > 1$, for the same reasons as discussed above. For upstream probability laws, one can use all datasets since the rigidities are well in the inertial range in the absence of compression effects. In what follows, we use different combinations of one downstream with one upstream of these datasets to simulate the Fermi acceleration process and measure the spectral index. We use these different datasets as independent realizations of the conditional probability laws in order to estimate the numerical uncertainty on the spectral index.

3.2 Escaping accelerated particles

The fraction of particles that do not return to the shock adds up to form the outgoing accelerated particle spectrum. As shown by Bell (1978) for the case of non-relativistic shocks, the spectral index of this spectrum is determined by the average return probability and the mean energy gain at each cycle. For relativistic shocks, the analytical development of Vietri (2002), whose formulation is very similar to that presented in Section 2, shows that the spectral index is determined by the energy gain properly averaged over the equilibrium distribution functions both upstream and downstream, see also Lemoine & Pelletier (2003).

The average energy gains per cycle u→d→u and half-cycles d→u, u→d are shown in Fig. 4, which shows clearly that the gain is of order $\simeq \Gamma_{\rm sh}^2$ for the first complete cycle u→d→u, and falls to $\lesssim 2$ in subsequent cycles, as anticipated by Gallant & Achterberg (1999), Achterberg *et al.* (2001). This strong limitation of the energy gain is due to the anisotropy of the distribution func-

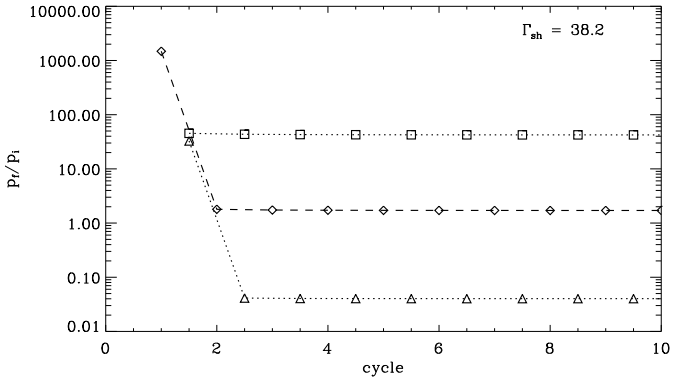

Figure 4. Average energy gain per cycle u→d→u (diamonds), per half cycle u→d (triangles), and per half cycle d→u (squares) plotted vs successive cycles.

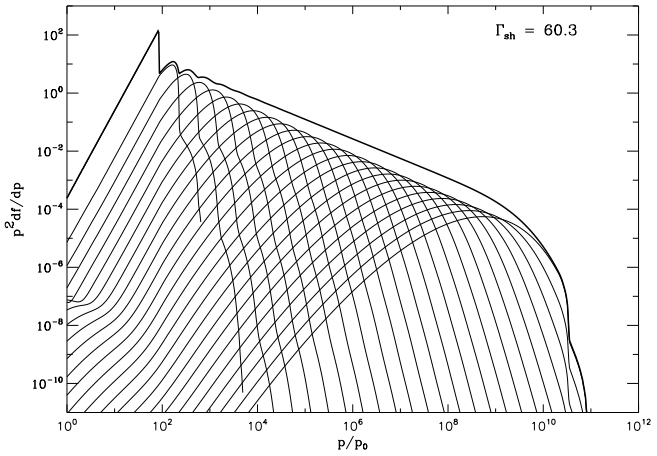

Figure 5. Accelerated spectrum of particles escaping downstream times momentum squared *vs* momentum (thick solid line); in thin solid lines, the accelerated populations that escape downstream at each cycle.

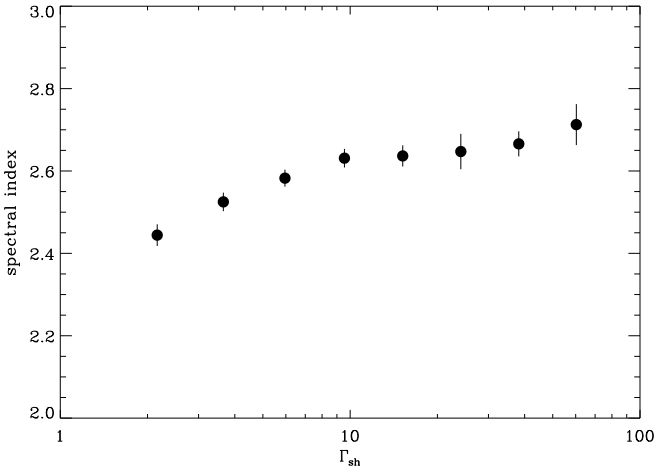

Figure 6. Spectral index *vs* shock Lorentz factor.

tion upstream: particles do not have time to be deflected by an angle greater than $\sim 1/\Gamma_{\rm sh}$ upstream before being overtaken by the shock which moves at speed $\beta_{\rm sh} \simeq 1$ with respect to upstream, hence the particles energy is decreased by a factor $1/\Gamma_{\rm rel}$ in the half-cycle u→d through the Lorentz transform, in agreement with Fig. 4. In order to return to the shock downstream, particles must turn back and the average energy gain in the half-cycle d→u is now $\simeq \kappa\Gamma_{\rm rel}$, with $\kappa \lesssim 2$ resulting in the total energy gain per cycle $\lesssim 2$. In the first cycle, the energy gain is large as the particle population injected upstream toward the shock is isotropic, hence in the first half-cycle u→d the energy gain $\sim \Gamma_{\rm rel}$.

The average energy gain per cycle u→d→u is $\langle p_{\rm f}/p_{\rm i}\rangle \simeq 1.7$ to within ± 0.1 for the various values of rigidity and shock Lorentz factor; this gain tends to diminish with increasing $\Gamma_{\rm sh}$ albeit with a weak slope. A similar behavior has been observed in the case of isotropic downstream turbulence (Lemoine & Pelletier 2003), the gain decreasing from $\simeq 2.0$ at $\Gamma_{\rm sh} = 2$ to $\simeq 1.9$ at $\Gamma_{\rm sh} \gg 1$.

Finally, using the method described in the previous section and the probability data collected during the Monte Carlo simulations, one can simulate the acceleration process itself and constructs the accelerated particle population. The result is presented in Fig. 5. This figure reveals that the sub-populations that escape at each cycle $2n+1$, and whose spectrum is roughly a gaussian centered on an energy $\sqrt{2}\Gamma_{\rm sh} p_0 g^n_{\rm u\to d\to u}$ (p_0 injection energy) and amplitude $\propto (1-\langle P_{\rm ret}\rangle)^n$, add up to form a featureless power law spectrum of index s (at $p \gg p_0$).

The measured spectral index s is shown as a function of shock Lorentz factor in Fig. 6. The comparison of these results with those obtained for isotropic scattering downstream shows that the inclusion of shock compression leads to a steeper accelerated spectrum at all values of $\Gamma_{\rm sh}$. One can understand this by noting that the compressed turbulence leads to lower average return probabilities and slightly lower energy gains than those obtained for isotropic turbulence (see Lemoine & Pelletier 2003).

The present results do not settle whether the spectral index reaches an asymptote at large shock Lorentz factors, but at the very least, as $\Gamma_{\rm sh} \gg 1$ it appears to evolve very weakly close to a value $s \simeq 2.6 - 2.7$.

3.3 Acceleration timescale

The present simulations provide a direct measurement of the acceleration timescale $t_{\rm acc}(\epsilon)$ at energy ϵ, which is defined as the u→d→u cycle timescale in the upstream rest frame divided by the mean energy gain:

$$t_{\rm acc}(\epsilon) \approx \frac{t_{\rm u|u}(\epsilon) + \Gamma_{\rm sh} t_{\rm d|d}(\epsilon/\Gamma_{\rm sh})}{g_{\rm u\to d\to u}}, \qquad (14)$$

where $t_{\rm u|u}$ and $t_{\rm d|d}$ are the upstream and downstream return timescales measured in their respective rest frames.

The upstream return timescale $t_{\rm u|u} \sim 10 t_{\rm L,u}/\Gamma_{\rm sh}$ ($t_{\rm L,u}$ upstream Larmor time) up to a weak residual dependency on the rigidity, as shown in Fig. 7. A fit that is accurate to a few percent over the range of rigidities and for $\Gamma_{\rm sh} \gtrsim 5$, is: $t_{\rm u|u} \simeq 14 t_{\rm L,u} \rho^{0.19}/\Gamma_{\rm sh}^{0.85}$. These results agree with and confirm the expectations of Gallant & Achterberg (1999) and Achterberg *et al.* (2001) who argued that $t_{\rm u|u} \propto 1/\Gamma_{\rm sh}$ since the particles are promptly overtaken by the shock when they have been deflected by an angle of order $1/\Gamma_{\rm sh}$.

The downstream return timescale is plotted *vs* rigidity for various shock Lorentz factors in Fig. 8. This figure shows that the return timescale $t_{\rm d|d} \approx 3 - 4R_{\rm L}/c$ at low rigidities $\rho \ll 0.1$ and $\Gamma_{\rm sh} \gg 1$. The uncertainty in the numerical prefactor contains a weak residual dependence on the shock Lorentz factor

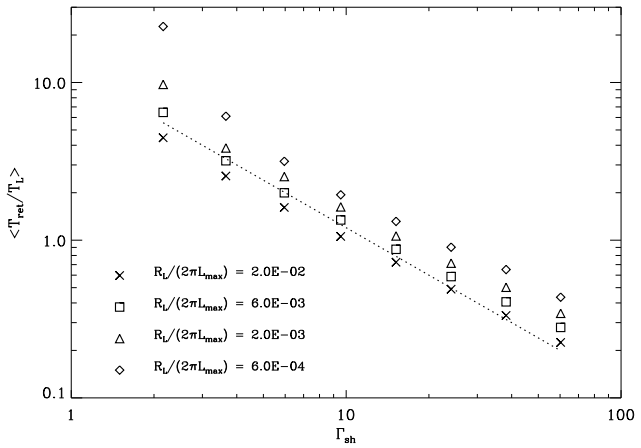

Figure 7. Upstream return timescale in units of Larmor time averaged over angular distribution *vs* shock Lorentz factor, for various rigidities as indicated. The dotted line $T_{\rm ret} = 12T_{\rm L}/\Gamma_{\rm sh}$ is shown as a guide the eye.

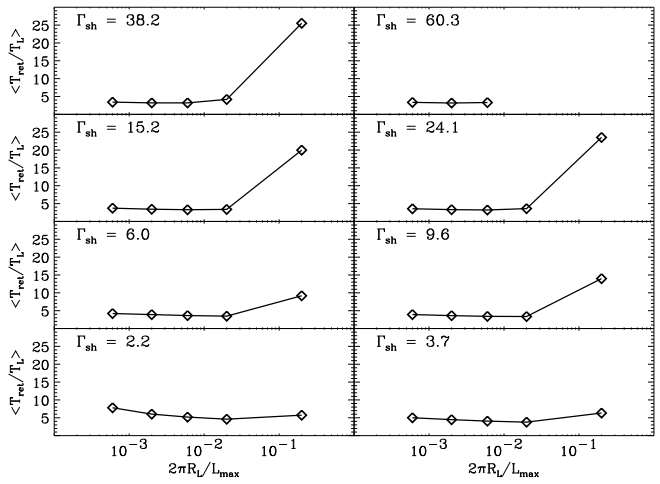

Figure 8. Downstream return timescale in units of Larmor time averaged over angular distribution *vs* rigidity for various shock Lorentz factors as indicated.

$t_{\rm d|d} \propto \Gamma_{\rm sh}^{-0.08}$ ($\Gamma_{\rm sh} \gg 1$). Note that for the moderately relativistic shock $\Gamma_{\rm sh} = 2.2$, the return timescale also contains a weak dependence on rigidity, $t_{\rm d|d} \propto \rho^{-0.13}$ approximately, which disappears at larger shock Lorentz factors. Here as well one can interpret the behavior of $t_{\rm d|d}$ as the result of reflections of particles on the compressed turbulence: the first scattering takes place on a Larmor timescale and flings the particles back to the shock with probability ≈ 0.3; if the particle does not return to the shock after this first scattering, the probability of doing so at subsequent scatterings becomes negligible for two reasons: the shock moves away at high velocity $\approx c/3$, and the enhancement of the tangential components of the magnetic field prohibits efficient transport along the shock normal.

At high rigidities, the downstream return timescale increases; the increase is all the more pronounced as the shock Lorentz factor is high. This is related to the difference between $\rho_\parallel$ and ρ; as $\Gamma_{\rm sh}$ increases, at a fixed value $\rho \sim 0.1$, the effective $\rho_\parallel$ becomes larger than $0.1-1$ and the particles leave the range where resonant scattering with turbulence modes along the shock normal is possible. The scattering time thus increases, see Section 4.1, and so does the return timescale.

Finally, the downstream return timescale can be written as $t_{\rm d|d}(\epsilon/\Gamma_{\rm sh}) \simeq 4R_{\rm L,d}(\epsilon/\Gamma_{\rm sh})/c \simeq \sqrt{3}R_{\rm L,u}(\epsilon)/\Gamma_{\rm sh}^2$, since the magnetic field strength is amplified by $\sqrt{2/3}R$. Hence the downstream return timescale measured in the upstream rest frame is slightly smaller than the upstream return timescale, and the total acceleration time: $t_{\rm acc} \approx 10R_{\rm L|u}/\Gamma_{\rm sh}$. Interestingly, the acceleration timescale becomes a fraction of a Larmor time at large shock Lorentz factor, which may allow acceleration to an energy limited by confinement arguments, in particular $R_{\rm L} \lesssim L_{\rm max}$, rather than by energy losses.

4 DISCUSSION

4.1 Relaxation length and transport in anisotropic turbulence

The present study has hitherto assumed that the downstream turbulence is successfully described by the direct compression of the upstream turbulence through the shock jump conditions. However one must expect this anisotropic compressed turbulence downstream to relax on a timescale $\tau_{\rm rel}$ (defined in the downstream rest frame), hence on a length scale $l_{\rm rel} = \beta_{\rm sh|d} c\tau_{\rm rel}$ downstream. Particles will then experience this compressed turbulence during their journey downstream provided the average distance traveled from the shock front $l_{\rm tr} \sim t_{\rm d|d}/2 \lesssim l_{\rm rel}$, or

$$t_{\rm d|d} \lesssim 2\beta_{\rm sh|d}\tau_{\rm rel}. \qquad (15)$$

Otherwise the particles reach the point where the turbulence anisotropy has relaxed and the previous considerations do not hold; however, as we now argue, the above inequality is generally satisfied in relativistic shocks for which the magnetic field is dynamically unimportant.

As discussed in Section 4.3, the return timescale $t_{\rm d|d} \approx 3 - 4R_{\rm L}/c$ for $\Gamma_{\rm sh} \gg 1$ and $2\pi R_{\rm L}/L_{\rm max} \ll 1$. There is a residual powerlaw dependence on both rigidity and shock Lorentz factor but whose power indices are < 0.1, see Section 3.3, which we can neglect for now. A simple but somewhat naïve estimate for the (scale dependent) relaxation timescale is $\tau_{\rm rel} \sim (kv_{\rm A})^{-1}$, where $k = 2\pi/l$ is the eddy wavenumber (related to the eddy size l), and $v_{\rm A}$ is the Alfvén velocity. Since particles of Larmor radius $R_{\rm L}$ diffuse through resonant interactions with turbulent modes of wavenumber $k \approx 1/R_{\rm L}$, the effective relaxation timescale to be considered is $\tau_{\rm rel} \sim R_{\rm L}/v_{\rm A}$. The inequality Eq. 15 is thus satisfied when $v_{\rm A}/c \lesssim 0.2$ (for $\Gamma_{\rm sh} \gg 1$), which agrees with the hypothesis made in Section 2 that the magnetic field is dynamically unimportant. Interestingly, one may show that the bound on $v_{\rm A}$ is more stringent for non-relativistic shocks, since the return timescale (for isotropic scattering at least) scales as $t_{\rm d|d} \propto t_{\rm scatt}/\beta_{\rm sh|d}$ in that case.

The estimate for $\tau_{\rm rel}$ is likely to be conservative since the eddy turn over rate, which gives a refined estimate of the relaxation time on a scale k, reads: $\tau_{\rm t-o} \approx (kv_k)^{-1}$, where v_k is now the turbulent velocity on the scale k, which decreases with increasing k; for a Kolmogorov spectrum, $v_k \propto k^{-5/3}$. With this new estimate $\tau_{\rm rel} \sim (kv_{\rm A})^{-1}(kL_{\rm max}/2\pi)^{5/3}$, the previous condition on $t_{\rm ret}$ reads: $\rho \lesssim 0.02(\beta_{\rm sh|d}/v_{\rm A})^3$. Since $R_{\rm L} \sim L_{\rm max}/2\pi$ marks the maximal energy reached in all likelihood, due to loss of confinement for $\rho > 1$, inequality Eq. 15 is valid at all rigidities if $v_{\rm A} \lesssim 0.1c$. Particles that are accelerated at the shock wave thus

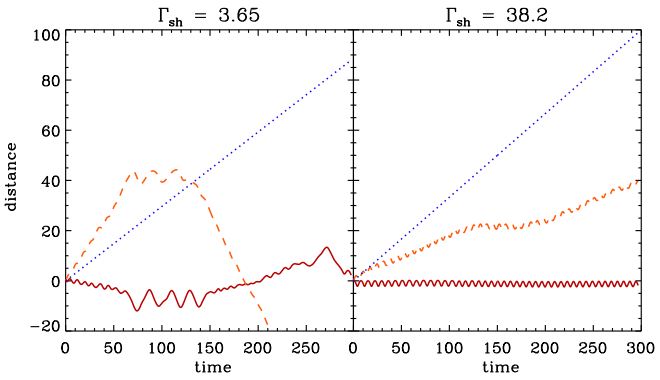

Figure 9. Typical trajectory for a particle propagating downstream in shock compressed turbulence with shock Lorentz factor $\Gamma_{\rm sh} = 3.7$ (left) and $\Gamma_{\rm sh} = 38$ (right). The dotted line indicates the trajectory of the shock front; the solid line shows the displacement along the shock normal while the dashed line gives the displacement in the plane parallel to the shock front.

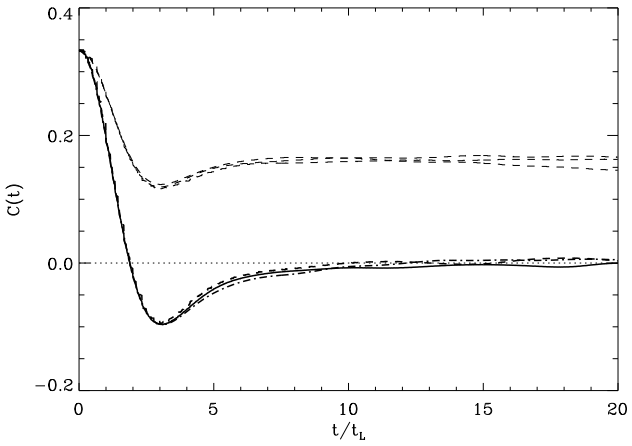

Figure 10. Velocity correlation function $C(\tau)$ *vs.* time (in units of Larmor time $t_{\rm L}$) for various values of rigidity ρ and shock Lorentz factor $\Gamma_{\rm sh}$. The lower thick curves correspond to the velocity oriented along the shock normal; in thick solid line, $\rho = 3 \cdot 10^{-6}$ and $\Gamma_{\rm sh} = 3.65$; in thick dashed line, $\rho = 3 \cdot 10^{-6}$ and $\Gamma_{\rm sh} = 38.2$; in thick dashed-dotted line, $\rho = 10^{-3}$ and $\Gamma_{\rm sh} = 3.65$. The upper dotted lines show the correlation function for the velocity components perpendicular to the shock normal; at $\tau \geqslant 15$, the upper two are $\rho = 3 \cdot 10^{-6}$ and $\Gamma_{\rm sh} = 3.65, 38.2$, the lower curve is for $\rho = 10^{-3}$ and $\Gamma_{\rm sh} = 3.65$.

do not travel far enough downstream to see anything else than the turbulence in its compressed state.

The transport of particles in strongly compressed turbulence is peculiar, as illustrated by Fig. 9. It presents examples of particle trajectories downstream for two different values of the shock Lorentz factor but for the same upstream magnetic configuration; in both cases the particle never returns to the shock. The comparison of the typical displacement along and perpendicular to the shock normal indicates that the particles appear confined in a layer of turbulence that lies tangential to the shock plane, and for periods of time extending well beyond a Larmor timescale. Note that for $\Gamma_{\rm sh} = 38$ (right panel), the particle appears to gyrate along a magnetic field line located in a plane parallel to the shock front. In this particular case, the magnetic field configuration is locally transverse. If the trajectory is followed for a sufficiently long period of time, it will depart from a simple Larmor gyration law. Moreover the effective pulsation is not constant along the trajectory shown in Fig. 9, but varies slightly in a random way. It is also apparent in these figures that the characteristic pitch angle scattering timescale along the shock normal is of order of a Larmor time, while that measured in the perpendicular direction is much larger. This demonstrates qualitatively how particles return to the shock in a few Larmor times by reflecting on the compressed turbulent modes.

In order to better characterize the transport of particles in compressed turbulence, one may seek the diffusion coefficients in the various directions. For our purposes, it is more relevant to study the time correlation function of the particle velocities, $C_{ij}(\tau)$:

$$C_{ij}(\tau) = \langle v_i(\tau) v_j(0) \rangle, \qquad (16)$$

where the average is to be taken on a large number of trajectories, and $v_i(\tau)$ is the velocity of the particle in the direction i at time τ. The integration of $C_{ij}(\tau)$ over τ leads to the diffusion coefficient D_{ij} (Candia & Roulet 2004). In the present case, the correlation function is however more relevant since particles never actually diffuse downstream before returning to the relativistically moving shock. The correlation functions along the shock normal, $C_{\parallel} = C_{zz}$ and perpendicular to the shock normal, $C_{\perp} = (C_{xx} + C_{yy})/2$ are shown for various values of $\Gamma_{\rm sh}$ and ρ in Fig 10. This figure demonstrates that the early time behavior of the parallel correlation function is, to a high degree of accuracy, independent of both $\Gamma_{\rm sh}$ and ρ, provided $\Gamma_{\rm sh} \gg 1$ and $\rho \ll 1$. The time behavior of $C_{\parallel}$ can be grossly approximated by $C_{\parallel}(\tau) \sim \cos(2\pi\tau/t_{\rm L}) \exp(-\tau/\tau_{\parallel})$, and $\tau_{\parallel}$ gives the scattering time along the shock normal. This fit is not reproduced on Fig. 10 for the sake of clarity, and because it diverges from the measured curves for $\tau/t_{\rm L} \gtrsim 10$. However, one can see by eye that the estimated $\tau_{\parallel} \approx 3 t_{\rm L}$.

On the contrary the velocities perpendicular to the shock normal do not decorrelate on timescales as short as $\tau_{\parallel}$; the fall-off of $C_{\perp}(\tau)$ toward zero is observed (but not shown on Fig. 10) on much longer timescales than $10 - 20 t_{\rm L}$, and the decorrelation time $\tau_{\perp}$ is found to depend on ρ. This is expected insofar as the scattering time in isotropic Kolmogorov turbulence $\tau_{\perp}/t_{\rm L} \propto \rho^{-2/3}$ (Casse *et al.* 2002). Indeed, in Fig. 10, the lower dashed curve corresponds to the high rigidity value, and it is seen to fall off more rapidly than the other two (that correspond to a same rigidity) at $\tau/t_{\rm L} \geqslant 15$. One may also note the slight decorrelation in perpendicular velocities induced at early times by the decorrelation of velocities along the shock normal.

This figure thus nicely explains the transport properties that were indirectly observed in the previous discussion, namely that the scattering time along the shock normal, which is the relevant quantity for shock acceleration, is of order of three Larmor times, and independent of rigidity and shock Lorentz factor to a good approximation.

4.2 Comparison to previous results

To our knowledge, there is no existing study of Fermi acceleration in ultra-relativistic shock waves which includes the effect of compression of the upstream magnetic field. One may nevertheless find interesting points of comparison in various limits with studies by Ballard & Heavens (1992), Ostrowski (1993), Bednarz & Ostrowski (1998), Kirk *et al.* (2000) and Niemiec & Ostrowski (2004).

Ballard & Heavens (1992) were the first to attempt modeling of Fermi acceleration in non-relativistic to moderately relativistic ($\Gamma_{\rm sh} \lesssim 5$) shocks with shock compressed turbulence by the means

of Monte Carlo methods. They found a pronounced steepening of the spectra index with increasing shock speed and derived the approximate formula $s \simeq 0.75\Gamma_{\rm sh} + 1.25$. Although our study confirms the increase of s with increasing values of $\Gamma_{\rm sh}$, the precise value of s differs significantly from those of Ballard & Heavens (1992), all the more so at large shock velocities. One may probably attribute this discrepancy to the modest dynamical range $(64-100)$ that was available at the time of the simulations of Ballard & Heavens (1992). If the dynamic range is not large enough, the particle rigidity always lie close to the upper range of resonance and this results in steeper spectra due to increased escape probability. The subsequent study by Ostrowski (1993) obtained much harder spectra than Ballard & Heavens (1992) where suitable comparison can be made. In particular, for large turbulence amplitude $\delta B/B = 3$, and shock Lorentz factors $\Gamma_{\rm sh} = (2.3, 5.0)$, Ostrowski (1993) obtained $s = (2.0-2.2, 2.2-2.3)$, where the range of values bracket different values of the mean field inclination with respect to the shock normal. Our results for s indicate slightly larger values for s, but the agreement is generally better than with Ballard & Heavens (1992).

Kirk *et al.* (2000) have studied relativistic Fermi acceleration using semi-analytical eigenfunction methods; their results confirm the canonical value $s = 2.23$ in the case of isotropic scattering. They have attempted to address the effect of anisotropic scattering downstream using an analytical description of compressed turbulence and an analytical estimate of the diffusion coefficient. They concluded that anisotropy does not affect significantly s, a result which is clearly at odds with the present study. The source of the discrepancy lies probably in the modeling of downstream diffusion by Kirk *et al.* (2000): as should be obvious from Figs. 10, particles propagating in strongly compressed turbulence downstream do not actually diffuse downstream but rather turn back by reflecting on a compressed magnetic layer.

The most detailed study to date is that of Niemiec & Ostrowski (2004), who have studied Fermi acceleration in moderately relativistic shocks ($\Gamma_{\rm sh} \lesssim 5$) by Monte Carlo integration of the particle trajectory in a magnetic field with a large dynamic range. Among the results obtained, the authors quote a generic non-power law behavior of the accelerated spectrum: the spectra generally appear harder close to the cut-off ($\rho \sim 1$) than well below the cut-off. Niemiec & Ostrowski (2004) conclude that this effect is probably related to the finite dynamic range: close to the cut-off, the propagation regime in compressed turbulence differs from that in the inertial range of resonance, and one indeed finds a different return probability or mean energy gain, both of which control the value of s. Our Fig. 5 reveals a smooth powerlaw behavior at energies well beyond the injection point; this is expected on the grounds that the conditional return probability histograms used to model Fermi acceleration is itself rigidity independent. We have demonstrated in the previous Sections that, deep in the inertial range $\rho \ll 0.1$, this is a good approximation; however, we have also observed that as ρ tends to larger values, the return probability reveals a slight dependence on ρ, and this would make s evolve with ρ, albeit for $\rho \gtrsim 10^{-2} - 10^{-1}$, had we included this dependence in our calculations.

Our results disagree markedly from those of Niemiec & Ostrowski (2004) with regards to the rigidity dependence of the return probability in the inertial range. These authors claim to observe a pronounced non-monotonic rigidity dependence, which is definitely absent from our simulations down to the percent level. We note that the noise level in the results of Niemiec & Ostrowski (2004) is not indicated in the figures, and might account for part of this apparent variability. On theoretical grounds, there is neither expectation nor justification for a rigidity dependence of $\langle P_{\rm ret}\rangle$ on ρ, as long as resonant interactions with the turbulence can occur and the shock lifetime is infinite. There is no clear explanation or interpretation of this observed rigidity dependence of the return probability in Niemiec & Ostrowski (2004). Furthermore their measured value of $\langle P_{\rm ret}\rangle$ does not agree with ours: for $\Gamma_{\rm sh} \simeq 5$ and $\delta B/B = 3$, they find $\langle P_{\rm ret}\rangle \simeq 0.20$, significantly lower than ours. This results in a steeper spectrum with $s \simeq 2.9 \pm 0.1$, to be compared with our value $s \simeq 2.6$; one should note that Niemiec & Ostrowski (2004) warrant caution with respect to their analysis of $\Gamma_{\rm sh} = 5$, as it lies close to the limits of their simulation capabilities.

We also note that the results of Niemiec & Ostrowski (2004) differ signicantly from those of Ostrowski (1993), although the method used is similar. For $\beta_{\rm sh} = 0.5$, $\delta B/B = 3$ and mean field inclination $\Psi = 45^o$, Niemiec & Ostrowski (2004) find $s = 2.7$ while Ostrowski (1993) obtains $s = 2.0 \pm 0.1$ for the same values (but $\Psi = 50^o$). This difference persists at larger inclinations, $s = 2.8$ in the former *vs* $s = 2. \pm 0.1$ in the latter for $\Psi = 75^o$, other values unchanged; it also persists at larger shock velocities, in particular for $\beta_{\rm sh} = 0.9$ ($\Gamma_{\rm sh} = 2.3$) and $\Psi = 45 - 50^o$, $s = 2.5$ in the former *vs* $s = 2. \pm 0.1$ in the latter. Here as well the source of the discrepancy remains unknown. Overall, and where comparison can be made, our results lie halfway between those of Ostrowski (1993) and those of Niemiec & Ostrowski (2004).

As stressed at the end of Section 2, the present method offers a significant gain in signal when compared to direct Monte Carlo methods but it cannot take into account the possible correlations between upstream and downstream trajectories due to the correlations between upstream and downstream magnetic fields at the point of shock-crossing. This remark, when taken together with the above comparison to previous work, shows the need for more exhaustive studies of relativistic Fermi acceleration with shock compressed turbulence, including mean magnetic fields of various strength and obliquity, and using both the present method and direct Monte Carlo methods.

4.3 Applications to astrophysical shock waves

Gamma−ray bursts, with their shock Lorentz factor in excess of 100 are ideal candidates to test theories on particle acceleration in ultra-relativistic flows. In the standard fireball model (see Meszaros 2002, Piran 2004 for reviews), the prompt $\gamma-$emission is interpreted as the product of synchrotron emission of electrons accelerated in the internal shocks with Lorentz factors $\Gamma_{\rm sh} \sim 2-5$ in the comoving wind frame. The afterglow emission is interpreted as the synchrotron light of electrons accelerated in the ultra-relativistic shock wave with $\Gamma_{\rm sh} \sim 300$, that itself results from the interaction of the $\gamma-$ray ejecta with its environment.

The spectral indices of the shock accelerated electrons derived in both cases are $s \simeq 2.3$. This has been interpreted as a dramatic confirmation of our understanding of relativistic Fermi acceleration since it agrees with the canonical value $s = 2.2$ obtained for isotropic downstream scattering. However, as should be clear by now, this "agreement" rather reflects our poor understanding of the acceleration process: the inclusion of shock compressed turbulence, which should be seen as a refinement of the theory, leads to steeper spectra, see Section 4, with $s \simeq 2.4 - 2.6$ for $\Gamma_{\rm sh} = 2 - 5$, and $s \simeq 2.6 - 2.7$ for $\Gamma_{\rm sh} \gg 1$.

The difference is not as significant in the case of internal shocks than for afterglow observations. As a matter of fact, isotropic scattering downstream predicts a value $s \simeq 2.1 - 2.2$

for $\Gamma_{\rm sh} = 2 - 5$ (Lemoine & Pelletier 2003), hence it could not account reasonably well for the dispersion observed in the spectral slopes of $\gamma-$ray prompt emission. However it is possible that the inclusion of a mean magnetic field component with varying inclinations and, possibly varying turbulence level, could reproduce this dispersion. Moreover it is not yet established whether the γ radiation results from synchrotron emission of shock accelerated electrons; other radiating processes (e.g. Piran 2004 and references therein) or magnetic reconnection events in the flow (e.g. Lyutikov & Blandford 2003) are likely possibilities.

Concerning the discrepancy of the present spectral index with that inferred from afterglow observations, one must note that the present study is limited to the case of pure Kolmogorov turbulence upstream, which idealizes the limit $\delta B/B \gg 1$. However, judging by the comparison with Niemiec & Ostrowski (2004), one does not expect the inclusion of a coherent component to help resolve this discrepancy, as these authors have observed a steepening of the accelerated spectrum with decreasing turbulence level $\delta B/B$. In the ultra-relativistic regime, this trend should be exacerbated, since as $\delta B/B$ decreases, one approaches the perpendicular shock acceleration limit where Fermi acceleration becomes inefficient (Begelman & Kirk 1990). Our simulations should thus provide a conservative lower bound to s for the case that includes a mean magnetic field.

The discrepancy might be attributed to the nature of the turbulence, in particular to the assumption of Kolmogorov turbulence. Again, the work of Niemiec & Ostrowski (2004) suggests that the turbulence spectral index has an effect on s, although there is not enough simulation data to pinpoint what the exact correlation is. These remarks indicate the need for more exhaustive studies that investigate various turbulence spectra. Interestingly, this suggests that prompt and afterglow observations of $\gamma-$ray bursts might be giving us information on the properties of the turbulence behind the shock front; the upstream turbulence does not play any rôle in the ultra-relativistic limit as a result of the limited amount of time that a particle spends upstream before being overtaken by the shock front.

The interpretation of $\gamma-$ray bursts afterglows as synchrotron emission by shock accelerated electrons requires that the magnetic field intensity at the shock front be significantly higher than the average interstellar value (e.g. Piran 2004 and references therein). The nature of downstream turbulence would then be directly related to the amplification process, which might manifests itself indirectly in the spectral slope. The proposal of magnetic field amplification by the two-stream Weibel instability (Medvedev & Loeb 1999) has recently triggered a lot of interest. This instability seems able of explaining the high value of B required, although debate on the subject is not closed, see Wiersma & Achterberg (2004). In any case, the Weibel instability amplifies the magnetic field in the transverse plane to the shock normal and on very small spatial scales (Medvedev & Loeb 1999) . If the magnetic field on scales larger than or equal to the Larmor radius of a typical accelerated particle is thus not amplified by the instability, one should expect acceleration to proceed as presented here, and the discrepancy should remain. These considerations may suggest that the amplified magnetic field structure differs from that proposed by Medvedev & Loeb (1999) or that the amplification mechanism itself is different. In this regard, we note that recent numerical studies on the Weibel instability suggests that powerlaw acceleration may occur independently of the Fermi mechanism due to the presence of electromagnetic currents downstream (Hededal *et al.* 2004). It should also be noted that stochastic acceleration in the downstream turbulence, which has not been accounted for in the present study, could play a significant rôle in reshaping the accelerated spectra, as suggested by Virtanen & Vainio (2005).

On a different line of thought, one should point out that the value of the spectral index derived here turns out to be in very good agreement with that required to fit the ultra-high energy part of the cosmic ray spectrum at energies $E \gtrsim 10^{18}$ eV, namely $s \simeq 2.6 - 2.7$, when one assumes that the sources are distributed at cosmological distances and do not evolve too strongly with redshift relatively to the cosmic star formation rate (Berezinsky *et al.* 2002, Berezinsky *et al.* 2005, Lemoine 2005).

5 SUMMARY

We have conducted a study of Fermi acceleration at relativistic and ultra-relativistic shock waves, considering the effect of the shock compression on the downstream magnetic turbulence. The numerical simulations are based on Monte Carlo methods of particle propagation in realistic magnetic fields described by sums of plane wave modes. The numerical technique differs from the standard Monte Carlo modeling of Fermi acceleration in that it measures the relevant statistical laws of particle transport on either side of the shock, and uses these probability laws together with the Lorentz transform from one frame to the other to reconstruct the acceleration process.

The turbulence was assumed to be described by pure Kolmogorov turbulence upstream, a situation which idealizes the limit $\delta B/B \gg 1$. The main effect of the compression with respect to the case of isotropic scattering is to steepen the accelerated spectrum to a slope $s \simeq 2.6-2.7$ in the limit $\Gamma_{\rm sh} \gg 1$, as a result of a decreased return probability. This latter effect is induced by the compression, which amplifies the magnetic field in the transverse direction to the shock normal: particles that enter downstream are trapped on a Larmor timescale in a compressed turbulence layer and cannot recross the shock unless they turn back within a few Larmor times. Consequently, the acceleration timescale is dominated by the usptream residence time, and can be as short as $t_{\rm acc} \simeq 10 t_{\rm L}/\Gamma_{\rm sh}$ (upstream frame). We have also argued that the accelerated particles do not travel far enough downstream before returning to the shock to experience a turbulence that has relaxed to near isotropicity.

The derived slope does not agree with that inferred from observations of $\gamma-$ray bursts afterglows, which indicate $s \simeq 2.3$. This inferred value is generally accepted as a success of Fermi acceleration in the relativistic regime whose predicted canonical value is $s \simeq 2.2 - 2.3$. However, this result only holds for isotropic scattering downstream, whereas the inclusion of realistic shock jump conditions, as done here, makes downstream turbulence strongly anisotropic and the spectra markedly steeper. The resolution of this discrepancy may be tied to the necessary but unknown amplification mechanism of the upstream magnetic field.

ACKNOWLEDGMENTS

We thank A. Marcowith and G. Pelletier for useful discussions and insight on the relaxation length of compressed turbulence.

REFERENCES

Achterberg A., Gallant Y. A., Kirk J. G., Guthmann A. W., 2001, MNRAS, 328, 393

Ballard K. R., Heavens A. F., 1992, MNRAS, 259, 89

Baring M., 2004, arXiv:astro-ph/0409303.
Bednarz J., Ostrowski M., 1996, MNRAS 283, 447.
Bednarz J., Ostrowski M., 1998, PRL, 80, 3911.
Bednarz J., Ostrowski M., 1999, MNRAS 310, L11.
Bednarz J., 2004, PASJ, 56, 923.
Begelman M. C., Kirk J. G., 1990, ApJ, 353, 66.
Bell A. R., 1978, MNRAS, 182, 147.
Berezinsky V., Gazizov A. Z., Grigorieva S. I., 2002, arXiv:hep-ph/0204357.
Berezinsky V., Gazizov A. Z., Grigorieva S. I., 2005, Phys. Lett. B, 612, 147.
Blandford R., McKee C., 1977, Phys. Fluids, 19, 1130.
Blasi P., Vietri M., 2005, arXiv:astro-ph/0503220.
Candia J., Roulet E., 2004, JCAP, 0410, 007.
Casse, F., Lemoine, M., & Pelletier, G. 2001, Phys. Rev. D, 65, 023002.
Ellison D. C., Reynolds S. P., Jones F. P., 1990, ApJ, 360, 702.
Ellison D., Double G. 2002, Astropart. Phys., 18, 213.
Ellison D., Double G., 2004, Astropart. Phys., 22, 323.
Gallant Y. A., Achterberg A., 1999, MNRAS, 305, L6.
Gallant, Y. A. 2002, in Relativistic Flows in Astrophysics, eds. A. W. Guthmann *et al.*, Lecture Notes in Physics (Berlin: Springer-Verlag), `arXiv:astro-ph/0201243`.
Gialis, D. & Pelletier, G., Astropart. Phys. in press, `arXiv:astro-ph/0302231`.
Hededal C. B., Haugboelle T., Trier Frederiksen J., Nordlund Å, 2004, ApJ, 617, L107.
Keshet U., Waxman E., 2005, PRL 94, 11102.
Kirk J. G., Schneider P., 1987, ApJ, 315, 425
Kirk J., Duffy P., 1999, J. Phys. G, 25, R163.
Kirk J., Guthmann A., Gallant Y., Achterberg A., 2000, ApJ, 542, 235.
Lemoine M., 2005, PRD, 71, 083007.
Lemoine M., Pelletier G., 2003, ApJ, 589, L73.
Lyutikov M., Blandford R. D., 2003, arXiv:astro-ph/0312347.
Medvedev M. V., Loeb A., 1999, ApJ, 526, 697.
Meli A., Quenby J. J., 2003, Astropart. Phys., 19, 637.
Meli A., Quenby J. J., 2003, Astropart. Phys., 19, 649.
Meszaros P., 2002, ARAA, 40, 137.
Niemiec J., Ostrowski M., 2004, ApJ, 610, 851.
Ostrowski M., 1991, MNRAS, 249, 551.
Ostrowski M., 1993, MNRAS, 264, 248.
Piran T., 2004, Rev. Mod. Phys., 76, 1143.
Peacock J., 1981, MNRAS, 196, 135.
Vietri M., 2002, ApJ, 591, 954.
Vietri M., 2003, arXiv:astro-ph/0304413.
Virtanen J. J. P., Vainio R., 2005, ApJ, 621, 313.
Waxman E., 1997, ApJ, 485, L5.
Wiersma J., Achterberg A., 2004, AA, 428, 365.